Journal of Physical Chemistry and Functional Materials

Home Page of Journal: https://dergipark.org.tr/jphcfum

Synthesis and characterization of Y-doped $ZnAl_2O_4$ spinels

Hanifi Kebiroğlu [1,*], *Ala Hamd Hssain* [2], *Bahroz Kareem Mahmood* [2], *Omer Kaygili* [1]

[1] *Department of Physics, Faculty of Science, Firat University, 23119, Elazig, Turkey*
[2] *Physics Department, College of Science, University of Halabja, 46018, Halabja, Iraq*

* *Corresponding author: Hanifi Kebiroğlu (hanifi007@hotmail.com)*

ABSTRACT

Zinc aluminum oxide ($ZnAl_2O_4$) type spinel samples doped with Y at various amounts of 0, 5, 10, and 15 at.% were produced and characterized for this study. Both X-ray diffraction (XRD) and Fourier transform infrared (FTIR) analyses confirmed the formation of the $ZnAl_2O_4$ phase for all the samples. For the spinels doped with Y at the amounts of 10 and 15 at.%, the formation of the secondary phase of Y_2O_3 was detected. The average crystallite size, lattice constant, unit cell volume, and crystallinity were affected by Y content, as well as the morphology.

ARTICLE INFO

Keywords:
Spinel;
Crystal structure;
Morphology

Received: 18-04-2021,
Accepted: 03-05-2021
ISSN: 2651-3080

1. INTRODUCTION

In terms of order and disorder, oxide spinels, which are a member of the ceramic family, are structurally rich materials [1]. Mg^{2+}, Fe^{2+}, Zn^{2+}, or Mn^{2+} occupy the tetrahedral site, and B is a trivalent cation occupying the octahedral site, such as Al^{3+} or Fe^{3+} [2-4]. A well-known form of normal spinel is zinc aluminate or zinc aluminum oxide ($ZnAl_2O_4$), which has a face-centered cubic structure. These spinels are made up of O^{2-} anions arranged by Zn^{2+} cations in the tetrahedral sites and Al^{3+} cations in the octahedral sites [1,3]. Aluminum (Al) spinels are refractory materials that range in color from semitransparent to translucent and from colorless to gray, blue, brown, and black.

Zinc aluminates are commonly used in a variety of technical fields, including the laser and ceramic industries [1-3,5-8]. Furthermore, these materials have a high irradiation tolerance, which is one of the most attractive characteristics for nuclear waste type materials [1].

Co-precipitation [9], combustion [10], hydrothermal route [1,3,11], solid-state synthesis [1], electrospinning [11], microemulsion [12], microwave [13], mechanochemical synthesis [14], and sol-gel [15] are some of the preparation methods for $ZnAl_2O_4$ spinels that have been recorded in the literature. Doping is a good way to get usable products with attractive properties, and lanthanides and transmission metal ions have been used as dopants to accomplish this [3,5,11,12].

2. Materials and method

In the wet chemical synthesis of the samples, zinc nitrate hexahydrate ($Zn(NO_3)_2{\cdot}6H_2O$), aluminum nitrate nonahydrate ($Al(NO_3)_3{\cdot}9H_2O$), and yttrium (III) nitrate hexahydrate ($Y(NO_3)_2{\cdot}6H_2O$) were used as the starting reagents and the distilled water was used as the solvent. The samples of $ZnAl_2O_4$, $ZnAl_{1.9}Y_{0.1}O_4$, $ZnAl_{1.8}Y_{0.2}O_4$, and $ZnAl_{1.7}Y_{0.3}O_4$ were prepared in this study. Using the nominal amounts of $Zn(NO_3)_2{\cdot}6H_2O$, $Al(NO_3)_3{\cdot}9H_2O$, and $Y(NO_3)_2{\cdot}6H_2O$ for each sample, the as-required solution was prepared in a flask having the volume of 100 mL. Afterward, the solution was poured into a beaker, and 10 mL of 0.5 M citric acid solution was dropped in this solution for each sample. The new solution was mixed in a magnetic stirrer at 80 °C for 3 h and was dried in an oven at 120 °C for 16 h. The as-dried powders were heated in an electric furnace at 1000 °C for 2 h.

A Bruker D8 Advance X-ray diffractometer was used to characterize the crystal structure of the as-produced spinel samples in the 2θ range of 20° - 80°

having a step size of 0.02° using CuKα radiation. A PerkinElmer Spectrum One spectrometer to record Fourier transform infrared (FTIR) spectra of the samples within the wavenumber range of 400-4000 cm^{-1} using the KBr method. The morphological investigations were carried out using a LEO EVO 40xVP scanning electron microscope (SEM) equipped with a Röntech xflash energy dispersive X-ray (EDX).

3. Results and discussion

3.1. XRD results

Fig. 1 shows the X-ray diffraction (XRD) patterns of the spinel samples. For all the samples, the existence of cubic zinc aluminum oxide or gahnite ($ZnAl_2O_4$, JCPDS Pdf no: 05-0669) phase was observed. For the first two samples, no additional phase was observed. At the higher Y contents, the formation of the secondary phase of yttrium oxide (Y_2O_3, JCPDS PDF No: 79-1716) was detected. The higher Y content caused the higher Y_2O_3 content, as seen from the results given in Table 1.

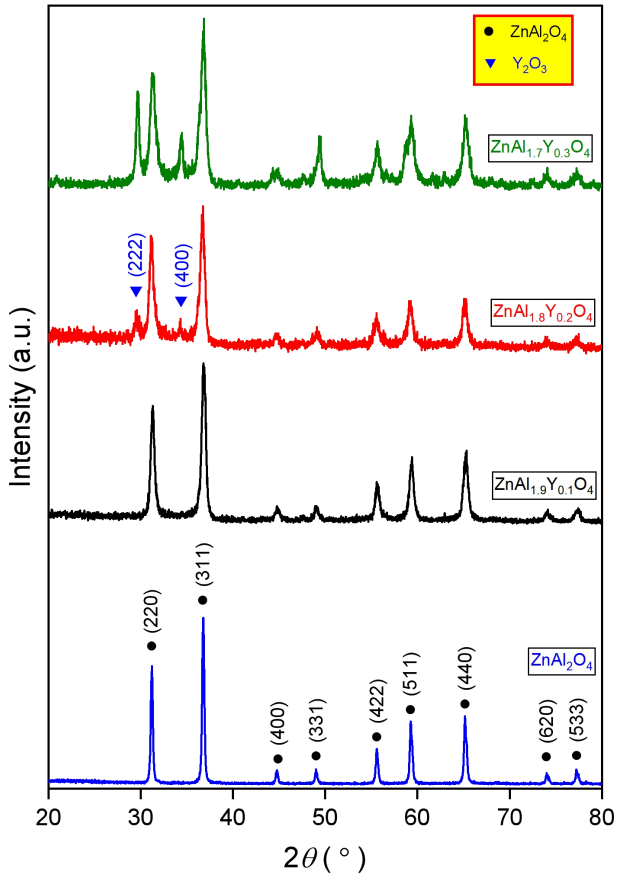

Fig. 1. XRD patterns of the un-doped and Y-doped samples

Using the as observed data belonging to the diffraction peaks of (220), (331), (400), (331), (442), (511), (440), (620) and (533) for the $ZnAl_2O_4$ phase, the average value of the crystallite size (t) for each spinel was calculated using the following Scherrer equation [16]:

$$t = \frac{0.9\lambda}{\beta \cos\theta} \quad (1)$$

here λ is the wavelength of incident X-rays, β is known as the full width at half maximum, and θ is the Bragg angle. The estimated values of this parameter were listed for each sample in Table 1.

The lattice parameter (a), unit cell volume (V), and crystallinity percent (X_C%) were calculated using the following relations, respectively [16, 17]:

$$a = d\sqrt{h^2 + k^2 + l^2} \quad (2)$$

$$V = a^3 \quad (3)$$

$$X_C\% = \frac{\sum A_C}{\sum A_C + \sum A_A} \times 100 \quad (4)$$

here h, k, and l are the Miller indices, d is the interplanar distance, and corresponds to the total areas under the crystal and amorphous peaks, respectively. As can be seen from the results in Table1, the average value of the crystallite size decreases with the increasing Y amount. The crystallinity is affected by Y-content. The crystallinities of the Y-doped spinel samples were found to be lower than that of the un-doped sample. The lattice parameter and unit cell volume were also affected by the amount of Y.

3.1. FTIR results

FTIR spectrum for each spinel sample is illustrated in Fig. 2. For all the samples, there are three detected bands in their FTIR spectra. The as-observed band positions are also listed in Table 2. The addition of Y affects the band position and causes some shifts, indicating the influence of the additive of Y into the spinel structure, to the higher wavenumber positions. All these three bands are related to the $ZnAl_2O_4$ structure and assigned to the vibrational modes of the Zn-O (first), O-Al-O (second), and Al-O (third) bonds, respectively [18-20]. The second and third bonds are related to the AlO_6 in the octahedral coordination state, verifying the formation of the $ZnAl_2O_4$ structure for each sample [21,22].

Table 1. The calculated values of the lattice parameter, unit cell volume, and average crystallite size of the samples

Sample	Phase composition (%)			t (nm)	X_C %	a (nm)	V (nm)^3
	$ZnAl_2O_4$	Y_2O_3					
$ZnAl_2O_4$	100	-		35	93.3	0.8098	0.531
$ZnAl_{1.9}Y_{0.1}O_4$	100	-		32.3	85.3	0.8094	0.5303
$ZnAl_{1.8}Y_{0.2}O_4$	93.9	6.1		27.7	83.2	0.8106	0.5236
$ZnAl_{1.7}Y_{0.3}O_4$	88.5	11.5		22	85.8	0.8085	0.5285

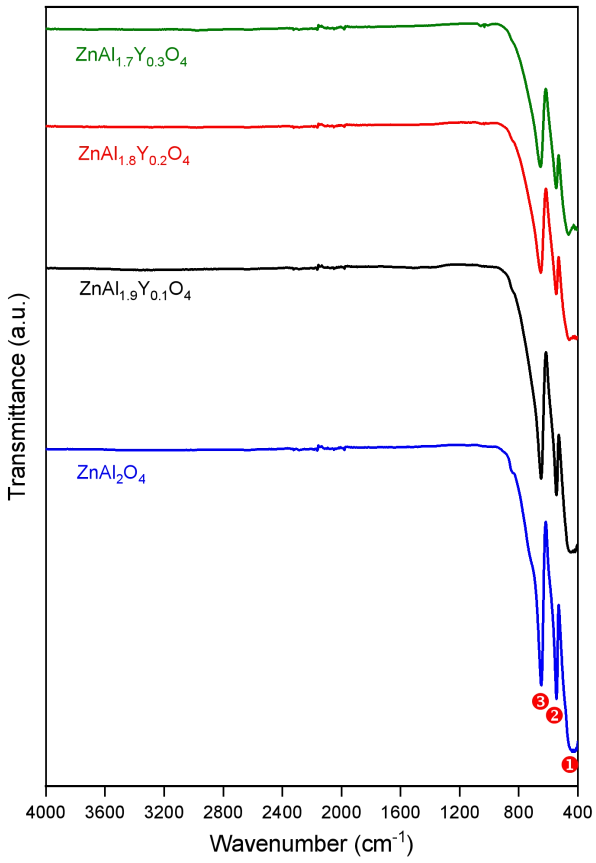

Fig. 2. FTIR results of the samples

Table 2. The as-observed band positions in FTIR spectra for all the samples

Sample	Band position (cm^{-1})		
	First	Second	Third
$ZnAl_2O_4$	451	545	648
$ZnAl_{1.9}Y_{0.1}O_4$	459	545	649
$ZnAl_{1.8}Y_{0.2}O_4$	459	547	651
$ZnAl_{1.7}Y_{0.3}O_4$	464	547	653

3.2. Morphological observations

The morphological investigation results taken from SEM and EDX analyses are shown in Fig. 3. Stacked plate-like grains containing pores in micron size were observed for all the samples. For the samples of $ZnAl_{1.8}Y_{0.2}O_4$ and $ZnAl_{1.7}Y_{0.3}O_4$, the sphere-like nanoparticles on these plate-like surfaces were detected. The addition of Y into the spinel structure affected the morphology. The EDX reports verified the purity of the samples and confirmed the influence of Y into spinel structure at increasing amounts. But, the as-detected amount of Y was not excessive, that is, the penetration of Y was limited.

4. Conclusions

In this study, we investigated the effects of Y-doping on the crystal structure and morphology of the well-known spinel-type of $ZnAl_2O_4$ structure. Four $ZnAl_2O_4$ samples were prepared by a wet chemical method, and their characterizations were carried out by using XRD, FTIR, SEM, and EDX methods. With the addition of Y, the following results were observed. The average value of the crystallite size decreased gradually. The lattice parameter and therefore unit cell volume changed. Compared to the un-doped one, the lower crystallinity values for the Y-doped samples were found. Both FTIR and XRD results supported the $ZnAl_2O_4$ structure for each sample. For samples containing more than 5 at.% Y, the formation of the new phase of Y_2O_3 was observed. The morphological changes were observed, and the purity of the samples was found to be 100%.

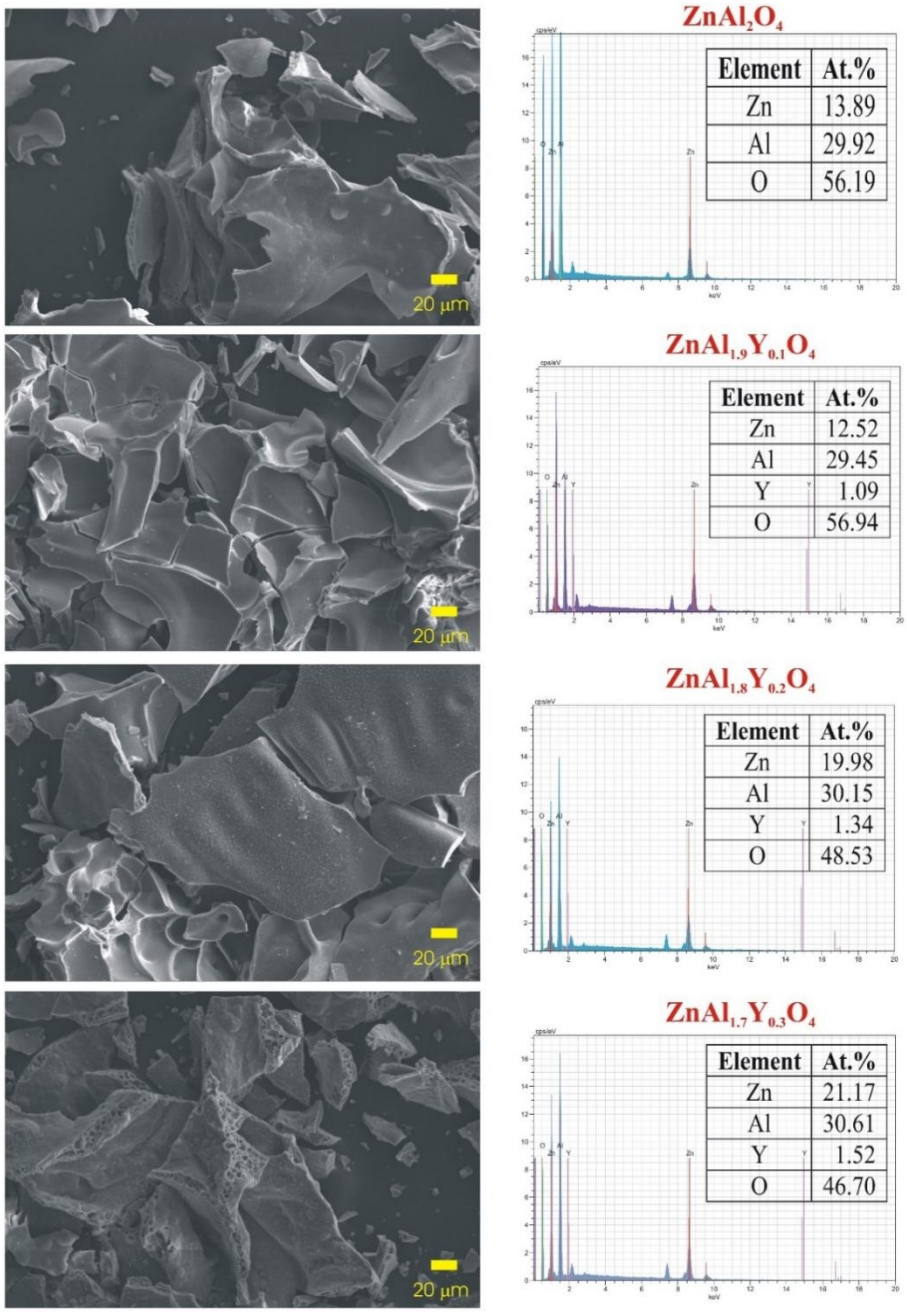

Fig. 3. SEM and EDX results of the as-produced spinel samples

References

[1] D. Dwibedi, C. Murugesan, M. Leskes and P. Barpanda, Role of annealing temperature on cation ordering in hydrothermally prepared zinc aluminate ($ZnAl_2O_4$) spinel, *Mater. Res. Bull.*, 2018, **98**, 219–224.

[2] M. Kumar and S.K. Gupta, An insight into optical spectroscopy of intense green emitting $ZnAl_2O_4$: Tb^{3+} nanoparticles: photo, thermally stimulated luminescence and EPR study, *J. Lumin*, 2015, **168**, 151–157.

[3] P. Kumari, Y. Dwivedi and A. Bahadur, Analysis of bright red-orange emitting Mn^{2+}: $ZnAl_2O_4$ spinel nanophosphor, *Optik*, 2018, **154**, 126–132.

[4] A. Belyaev, L. Basyrova, V. Sysoev, M. Lelet, S. Balabanov, V. Kalganov, V. Mikhailovski, M. Baranov, E. Stepanidenko, V. Vitkin, O. Dymshits and P. Loiko, Microstructure, doping and optical properties of Co^{2+}: $ZnAl_2O_4$ transparent ceramics for saturable absorbers: Effect of the ZnF_2 sintering additive, *J. Alloys Compd.*, 2020, **829**, 154514.

[5] M. Mohapatra, M. Kumar and R.M. Kadam, Trap level spectroscopic investigations of U: $ZnAl_2O_4$: Role of defect centres in the TSL process, *J Phys Chem Solids*, 2018, **114**, 83–87.

[6] S.F. Wang, Y.T. Tsai and J.P.Chu, Resistive switching characteristics of a spinel $ZnAl_2O_4$ thin film prepared by radio frequency sputtering, *Ceram. Int.*, 2016, **42**, 17673–17679.

[7] A. Movasati, S.M. Alavi and G. Mazloom, Dry reforming of methane over CeO_2-$ZnAl_2O_4$ supported Ni and Ni-Co nanocatalysts, *Fuel*, 2019, **236**, 1254–1262.

[8] R. Yang, A. Han, M. Ye, X. Chen and L. Yuan, The influence of Mn/N-codoping on the thermal

performance of $ZnAl_2O_4$ as high near-infrared reflective inorganic pigment, *J. Alloys Compd.*, 2017, **696**, 1329-1341.

[9] T.K. Parya, R.K. Bhattacharyya, S. Banerjee and U.B. Adhikari, Co-precipitated $ZnAl_2O_4$ spinel precursor as potential sintering aid for pure alumina system, *Ceram. Int.*, 2010, **36**, 1211–1215.

[10] R. Ianoş, R. Băbuţă, C. Păcurariu, R. Lazău, R. Istratie and C. Butaciu, Combustion synthesis of $ZnAl_2O_4$ powders with tuned surface area, *Ceram. Int.*, 2017, **43**, 8975–8981.

[11] Q. Pan, S. Ye, D. Yang, J. Qiu and G. Dong, Multifunctional magnetic-fluorescent Ni-doped $ZnAl_2O_4$ nanoparticles with second biological NIR window fluorescence, *Mater. Res. Bull.*, 2017, **93**, 310–317.

[12] D. Zhang, Y. Yin, Y. Liu, W. Chao and Y. Zhai, The photoluminescence and magnetic properties of $ZnAl_2O_4$: Mn nanocrystals, *J Phys Chem Solids*, 2013, **74**, 1131–1135.

[13] N. Peillon, F. Zuo, C. Meunier, S. Saunier, S. Marinel and D. Goeuriot, In-situ studies on preparation of $ZnAl_2O_4$ spinel using microwave reactive sintering technique, *Mater. Lett*., 2016, **167**, 77–80.

[14] A.D. Ballarini, S.A. Bocanegra, A.A. Castro, S.R. de Miguel and O.A. Scelza, Characterization of $ZnAl_2O_4$ obtained by different methods and used as catalytic support of Pt., *Catal. Lett*., 2009, **129**, 293–302.

[15] A.V. Belyaev, M.I. Lelet, N.I. Kirillova, N.M. Khamaletdinova, M.S. Boldin, A.A. Murashov and S.S. Balabanov, Sol-gel synthesis and characterization of $ZnAl_2O_4$ powders for transparent ceramics, *Ceram. Int.*, 2019, **45**, 4835–4839.

[16] O. Kaygili, N. Bulut, T. Ates, I. Ercan, S. Koytepe, T. Seckin, C. Tatar, B. Gunduz and H. Kebiroglu, Structural and thermal properties of Zn-containing magnesium aluminate spinels obtained by wet chemical method, *Mater. Sci.-Poland*, 2019, **37**, 238-243.

[17] O. Kaygili, Synthesis and characterization of Na_2O–CaO–SiO_2 glass–ceramic, *J. Therm. Anal. Calorim*., 2014, **117**, 223–227.

[18] P.K. Haldar, S. Dey, S. Mukhopadhyay and T.K. Parya, Structural and optical properties of Ti^{4+} doped sintered $ZnAl_2O_4$ ceramics, *Interceram. - Int. Ceram. Rev*., 2014, **63**, 382–385.

[19] T.S. Nirmala, N. Iyandurai, S. Yuvaraj and M. Sundararajan, Effect of Cu^{2+} ions on structural, morphological, optical and magnetic behaviors of $ZnAl_2O_4$ spinel, *Mater. Res. Express*, 2020, **7**, 046104.

[20] M.K. Habibi, S.M. Rafiaei, A. Alhaji and M. Zare, $ZnAl_2O_4$: Ce^{3+} phosphors: Study of crystal structure, microstructure, photoluminescence properties and efficient adsorption of Congo red dye, *J. Mol. Struct*., 2021, **1228**, 129769.

[21] W. Mekprasart, K. Boonyarattanakalin, W. Pecharapa and K.N. Ishihara, Optical characteristics of samarium doped $ZnAl_2O_4$ nanomaterials synthesized by vibrational milling process, *Mater. Today-Proc*., 2018, **5**, 14126–14130.

[22] W. Staszak, M. Zawadzki and J. Okal, Solvothermal synthesis and characterization of nanosized zinc aluminate spinel used in iso-butane combustion, *J. Alloys Compd*., 2010, **492**, 500–507.